Self-Sensing Induction Motors for Condition Monitoring

Christopher J. Schantz and Steven B. Leeb

Abstract— **Motors have been exploited as their own sensors for diagnostic and operating conditions at least, since the dawn of modern computing. Contracting systems theory offers a new level of precision in detecting small parameter and state changes in an electric machine for load fault detection and diagnostics from the motor terminals. The presented offline method successfully solves the motor inverse problem to reconstruct the characteristic instantaneous angular speed and load torque signals of the motor during periodic operation. The solution includes a motor parameter estimation step that reflects the specific temperatures and magnetic saturation of the motor during data acquisition. This identification or inversion method is suitable for induction motors driving periodic loads with and without rotor angle-dependent loading. A practical condition monitoring application is demonstrated: valve and cylinder fault detection in reciprocating compressors.**

Index Terms— **Condition monitoring, fault detection, induction motors, parameter estimation, signal reconstruction.**

I. Introduction

MORE than 300 million industrial electric motors are installed worldwide [1], and many more in non-industrial settings. Electromechanical sensors for machine shaft operation are often essential for diagnostics and control. However, sensors can add expense and a failure point. Every motor is influenced by the torque and speed characteristics of its load. This means that information about the mechanical state of the motor's load is potentially available from the motor electric terminals. In this work we generalize a contraction-based model inversion method [2] to a new class of periodic loads that are not dependent on rotor angle. The method turns the motor with a periodic load into a high fidelity virtual speed and torque sensor using easy to measure electric signals, i.e., signals that are often already available in an industrial or commercial application, by reconstructing fine variations of rotor speed $\omega_r(t)$ and motor electromagnetic torque $\tau_e(t)$ on time scales shorter than the motor shaft rotation period. The offline method obtains a level of precision distinct from most other sensor-less methods by taking advantage of powerful non-casual data filtering and processing. Economical electric sensors and computation can replace costly mechanical sensors for a host of fault detection and diagnostics applications of motor driven machinery.

The technique reconstructs high quality motor speed and torque signals by inverting the 5^{th} order induction motor model [3]. Data preprocessing removes noise and other signal content such as space and time harmonics due to non-ideal motor construction. Prior knowledge of the motor's parameters (resistances and inductances) is not required because the parameters are jointly estimated from the same data used for $\omega_r(t)$ and $\tau_e(t)$ estimation, ensuring they reflect the motor temperature and magnetic saturation level. The primary requirement is that the motor is operating at least briefly in a periodic steady state, where average shaft speed $\bar{\omega}_r$ and load torque $\bar{\tau}_l$ are quasi-steady state on time scales greater than the motor shaft rotation period. The inversion technique presented here is in principle applicable to other types of periodically driven electromagnetic actuators, but we focus on the induction motor in this paper.

II. Monitoring the Load From the Motor Terminals

A. Related Work

Using an actuator as its own sensor for fault detection and condition monitoring of electric machines has received considerable attention, see [4]–[7] for recent examples and [8]–[12] for five recent review papers. Reference [8] focuses mostly on motor current signature analysis (MCSA), a technique that examines the spectral signatures of motor currents for harmonics resulting from common motor pathologies, including rotor eccentricity, broken rotor bar, and bearing faults. Reference [9] surveys techniques applicable to medium voltage induction motors, while [10] reviews stator fault detection, and [11] reviews rotor fault detection. These reviews highlight that motor electrical currents contain a wealth of information about motor condition, and that the non-model based MCSA is a common method of reference for industrial applications [12]. Review [12] calls for further research on motor condition monitoring methods that are robust to load inertia and disturbances. For load condition monitoring, however, we require an algorithm that seeks to make the motor transparent to the load.

The load fault or effect has sometimes been treated as a disturbance to motor condition monitoring [13], [14]. Load faults like unbalance or mis-alignment have also been treated similarly to motor faults like rotor eccentricity [15]. An early example was [16], which used MCSA to monitor motor operated valves in power plants. Gear and gear box condition

Manuscript received March 20, 2017; revised April 23, 2017; accepted April 23, 2017. Date of publication May 2, 2017; date of current version May 22, 2017. This work was supported in part by the Grainger Foundation and in part by the ExxonMobil-MIT Program through the MIT Energy Initiative. The associate editor coordinating the review of this paper and approving it for publication was Prof. Boby George. *(Corresponding author: Christopher J. Schantz.)*

The authors are with the Department of Electrical Engineering and Computer Science, Massachusetts Institute of Technology, Cambridge, MA 02139 USA (e-mail: cschantz@mit.edu; sbleeb@mit.edu).

Digital Object Identifier 10.1109/JSEN.2017.2700386

monitoring through motor current represents a related active area of research, [17]–[21]. [18] explains the appearance of gear fault frequencies in the voltage and current spectra of brushless DC motors via amplitude modulation. The authors of [19], [20] present methods to improve the signal to noise ratio of gear fault frequency detection in motor current spectrums obscured by disturbances and supply line noise. The discrete wavelet transform [19], and frequency demodulation [20], are applied to the motor stator currents prior to Fourier spectrum computation. An analytical interpretation of stator current is taken in [21] and [22], where gear properties like transmission error and torsion stiffness variation are first translated to load torque oscillation models, before using an expanded magnetomotive force and permanence wave analysis to determine the effect on stator currents. Reference [21] derives and validates a multi-component phase modulation model for the load effect on stator currents, using an experimental platform. References [23]–[25] assume load faults are represented by generic load torque oscillations, determine the effect on the stator currents, and apply time frequency analysis to track load condition, including power spectral densities, instantaneous frequency (IF) estimation, and Wigner distributions.

One important draw-back to the majority of these MCSA-related methods is the assumption that a load fault is adequately modeled by an oscillation in load torque about its mean value. Tracking characteristic fault frequency magnitudes also increases the difficulty of interpreting the fault symptoms for fault diagnosis, especially for the large class of loads for which variable load torque fluctuations are part of nominal operation. Examples of such loads are positive displacement pumps, where torque pulsations depend strongly on their (possibly variable) operating pressure differential.

Model based approaches, like the one presented here, clarify the parameter and source of a pathology or operating condition. The proposed method, like many others, uses measured stator currents and voltages to estimate electromagnetic torque [26]–[32] or speed [33], [34], avoiding the need for time frequency processing of the stator current waveforms. Generally, the literature of torque estimation for load condition monitoring assumes a static or average shaft speed to justify the electromagnetic torque $\tau_e(t)$ as a substitute for the load torque $\tau_l(t)$, which in our application includes all non electromagnetic torques, such as motor and load friction components. Of course, $\tau_e(t)$ is essentially never equal to the $\tau_l(t)$ excepting in steady state (when it will then carry little useful information) due to the inertia torque of the rotating elements. Because the load condition information is carried in load torque oscillations, methods which assume a steady state condition, even if only to make the $\tau_e(t) = \tau_e(t)$ substitution, are limited in diagnostic power and accuracy, especially in situations with periodically varying shaft speeds. Computing $\tau_l(t)$ from $\tau_e(t)$, (1), requires sufficiently precise shaft speed estimates, $\omega_r(t)$, to be differentiable to find the rotational acceleration and inertia torque, as we obtain here. Inertia J is presumed known for the monitored motor and load.

$$\tau_l(t) = \tau_e(t) - J\dot{\omega}_r(t) \tag{1}$$

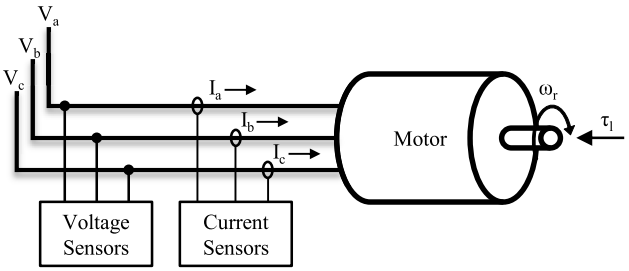

Fig. 1. Induction motor and electric sensors.

Reference [34] estimated the shaft speed of a fan by tracking rotor slot harmonics in the motor stator currents [35], [36]. Shaft speed was compared to the characteristic fan curve of the ventilation fan to monitor air flow velocity for filter clogging or duct leak detection, again essentially reducing speed estimation to a static steady state condition that does not exist experimentally. Here, we also optionally use rotor slot harmonics for longer time scale shaft speed estimation as part data pre-processing. Induction motor dynamics driving periodic loads were explored in [37]–[39] by reformulating the motor model into a system of algebraic Fourier coefficient equations. This was limited to being an analysis tool, and did not pose an inverse problem.

B. Motor Inversion

Wall fed three phase induction motors are supplied with inputs of stator voltage and shaft load torque $\tau_l(t)$. In response, the motor draws current and develops an electromagnetic torque $\tau_e(t)$, This is the forward problem, shown in Fig 1. If $\tau_l(t)$ is periodic in time or in shaft angle, then the motor will operate in periodic-steady state and subsequently $\omega_r(t)$, $\tau_e(t)$, and the motor current will be periodic. In periodic steady state, the inverse problem uses a nearly noise free "characteristic period" of measured stator currents and voltages to reconstruct $\omega_r(t)$ and $\tau_e(t)$, with enough fidelity to perform numerical differentiation to solve (1) for $\tau_l(t)$. The fine variation in instantaneous angular speed $\omega_r(t)$ and load torque $\tau_l(t)$ contain a wealth of information on the condition of the driven load.

III. Method Framework

Inverse problems are sensitive to noise, un-modeled signal content, and parameter error [40]. We remove noise and un-modeled dynamics from the measured signals by synchronous averaging on the load periodicity. The induction motor's model is a contracting system, [41], and therefore responds to periodic inputs with periodic outputs (permitting the appearance of higher harmonics), a corollary of the contraction property, [42]. As the loading becomes less periodic, the strength of the periodic content in the measured signal diminishes relative to the noise and unmodeled dynamics, and the synchronous averaging periods become harder to define, thereby creating challenges for the application of the method to strongly continuous loads or transient fault conditions. Successful synchronous averaging requires a data

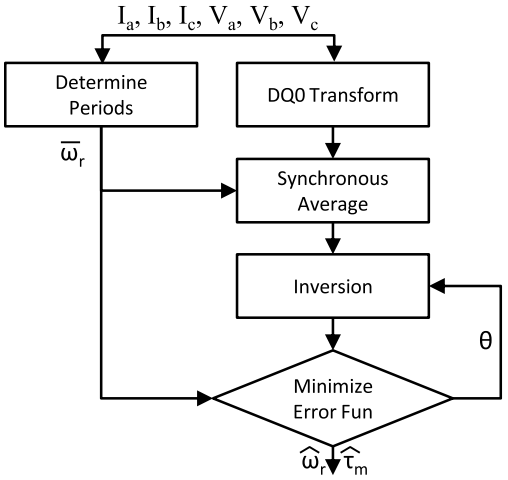

Fig. 2. Inversion algorithm flow chart.

record containing enough averaging periods to remove noise and non-periodic harmonics, but not so many that neglected factors like thermal drift in resistances start to matter. The motor inversion with the synchronously averaged currents as inputs gives single periods of $\omega_r(t)$ and $\tau_e(t)$ that do not correspond to any particular period of operation, but rather are characteristic of the periodic steady state of the motor. The major processing flow of the algorithm is shown in Fig. 2.

A. Data Preprocessing

Three- phase currents and voltages are sampled in the stationary "abc" frame, giving $\boldsymbol{i_a}$, $\boldsymbol{i_b}$, and $\boldsymbol{i_c}$, (Fig 3a) and $\boldsymbol{v_a}$, $\boldsymbol{v_b}$, and $\boldsymbol{v_c}$. Bolded quantities represent discrete time series. Sampling frequency, f_s, must be fast enough to record all significant harmonics of the constituent periodicities without distortion by anti-aliasing filters. Name plate data makes it straightforward to predict the approximate number of shaft rotations for a given recording duration for wall fed motors.

"Abc" quantities are then transformed to the dq0 reference frame, rotating synchronously with the utility frequency $\omega_e(t)$, which often drifts slightly during the recording. An estimate of $\omega_e(t)$ is obtained from the sampled voltages for a precise transform to prevent drift in $\boldsymbol{i_d}$ and $\boldsymbol{i_q}$. We used demodulation and IF estimation to compute $\omega_e(t)$, taking advantage of zero phase filters in the offline computation. The starting angle for the dq0 transform is chosen to insure no zero crossings in the $\boldsymbol{i_d}$ and $\boldsymbol{i_q}$, shown in Fig. 3b. This prevents later numerical problems during element-wise division.

$$\bar{\boldsymbol{x}}\left[n_p\right] = \frac{1}{\lfloor N/N_p \rfloor} \sum_{i=0}^{\lfloor N/N_p \rfloor - 1} \boldsymbol{x}\left[n_p + iN_p\right] \tag{2}$$

Synchronous averaging a signal $\boldsymbol{x}[n], n = 0, 1, \ldots N$ effectively implements a comb filter, passing only the mean, fundamental, and harmonics of the averaging period [43]. The result is a discrete vector of length N_p equal to one averaging period: $\bar{\boldsymbol{x}}\left[n_p\right], n_p = 0, 1, \ldots N_p - 1$, using (2). The length of the data is given by N, and N_p is the number of points of the p^{th} periodicity with period T_p. For a fixed f_s it is unlikely that an integer number of samples will be collected every T_p. This leads to error when evaluating (2). To address this error, $\boldsymbol{x}[n]$ is interpolated to a higher sampling rate f_{sp}, given in (3), before averaging with (2). Interpolation to the higher sampling rate is achieved by zero padding in the frequency domain.

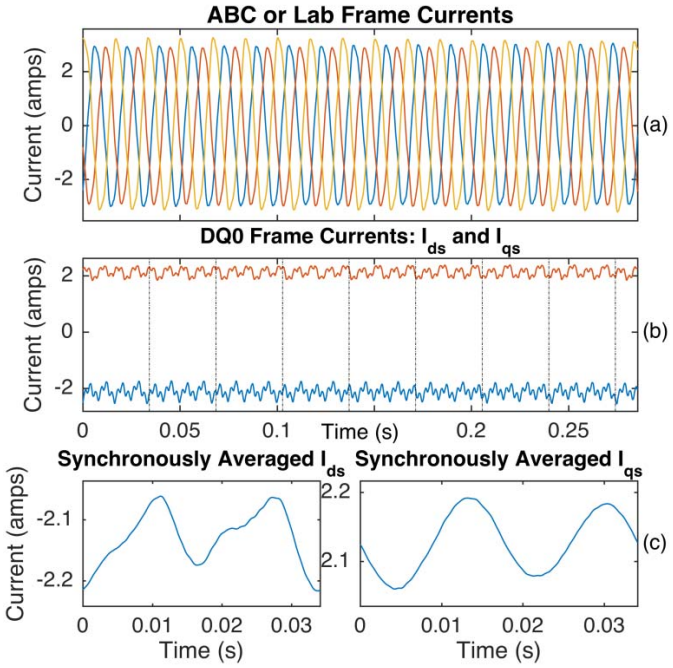

Fig. 3. (a) "abc" frame stator currents from wall-connected induction motor. (b) Stator currents in the dq0 frame, $\boldsymbol{i_q}$ and $\boldsymbol{i_d}$. Zero axis currents are negligible and not shown. (c) One period of synchronously averaged $\boldsymbol{i_d}$ and $\boldsymbol{i_q}$. Averaging has removed all utility frequency harmonics. Only content at the shaft period and its harmonics remains.

$$f_{sp} = \frac{\lceil f_s T_p \rceil}{T_p} \tag{3}$$

In a multi-periodic case with P periodicities, synchronous averaging separates the signal into its constituent periods. This is important for the frequency domain portion of the inversion equations solution, to be discussed later.

Electric motors are subject to periodic inputs from different sources. Internal sources include higher order non-symmetric construction asymmetries. In many machines, e.g. direct drive pumps, the load torque is a function of the rotor angle, repeating every shaft rotation. This periodicity is coincident with any torque ripple caused by the motor's asymmetric construction, and considered a singly-periodic case. To the extent that non-sinusoidal winding distributions, finite rotor and stator slots, rotor eccentricities, and so on lead to periodic current ripples, the synchronous averaging and inversion algorithm preserves and accounts for these effects in the resulting speed and torque estimates. Machines with transmission ratios such that the load periodicity is an integer harmonic of the rotor speed (or vice versa) are also treated as singly periodic with the longest period. Multi-periodic cases arise when the load torque is either modulated by a periodic influence not related to rotor speed or from non-integer transmission ratios in the load machinery.

The periods of the load torque must be known to synchronously average $\bar{\boldsymbol{i}}_{\boldsymbol{d}}\left[n_p\right]$ and $\bar{\boldsymbol{i}}_{\mathbf{q}}\left[n_p\right]$, Fig 3c. Effective

methods to determine mean motor shaft speeds from the motor currents electric signals, i.e. rotor slot harmonic tracking, exist [34]–[36]. Moreover, periodic loads often draw significant current at the load frequency, and a straightforward spectrum of the motor currents will easily reveal a dominant spike at the shaft rotation frequency. Load design parameters like transmission ratios are also useful sources for determining the required periods from the average motor shaft speed. Thus the necessary synchronous averaging period(s) and the required mean shaft speed for the parameter estimation in section D are determined from the motor currents, preserving the electric sensor only, non-intrusive nature of the algorithm.

B. Motor Model and Inversion Equations

To present the fifth order induction motor model, we take advantage of the orthogonality of the direct (D) and quadrature (Q) axes and write the equations with complex variables, where the D axis is aligned with the real axis, and the Q axis is aligned with the imaginary axis. Subscripts denote either rotor (r) or stator (s) quantities, and j is the imaginary number. The motor model, in terms of flux linkages λ is stated according to (4)–(6). $v_s$is the stator voltage, i_s the stator current, ω_r the rotor speed, ω_e the electrical supply frequency, and τ_l the load torque, which includes all frictions that may be present in the motor or load.

$$\dot{\lambda}_s = v_s - R_s i_s - j\omega_e \lambda_s \tag{4}$$

$$\dot{\lambda}_r = j\left(\frac{P_m}{2}\omega_r - \omega_e\right)\lambda_r - R_r i_r \tag{5}$$

$$\dot{\omega}_r = \frac{1}{J}\left(\frac{3L_m P_m}{4D}\mathbf{Im}\left\{\lambda_s^* \lambda_r\right\} - \tau_l\right) \tag{6}$$

Stator and rotor currents defined in (7) and (8).

$$i_s = \frac{L_{ar}\lambda_s - L_m \lambda_r}{D} \tag{7}$$

$$i_r = \frac{L_m \lambda_s - L_{as}\lambda_r}{D} \tag{8}$$

The model parameters are the stator (R_s) and rotor (R_r) resistances, the magnetizing inductance L_m, and the total stator (L_{as}) or rotor (L_{ar}) inductance. The D parameter is a convenience defined in terms of inductances according to (9), and has a negative value. P_m is the pole count of the machine. $\mathbf{Im}(\cdot)$ is the imaginary part operator, and * indicates conjugation. J is the rotor inertia.

$$D = L_m^2 - L_{as}L_{ar} \tag{9}$$

The first inversion equation, (10), solves for $\mathbf{\Lambda_s}\left[k_p\right]$ as a function of v_s and $\bar{\boldsymbol{i}}_{\boldsymbol{s}}[n_p]$ and is derived by Fourier transform of (4). $\mathcal{F}\{\cdot\}$ is the Discrete Fourier Transform (DFT) operator. The result of (10) is the motor's stator flux. Fourier methods enforce solutions with periodic boundary conditions; meaning (10) is a natural choice for the periodic, synchronously averaged motor currents. Capitalized variables and bracket index k_p signify a frequency domain vector. (10) is similar to the well-known stator flux estimation in the synchronous reference frame by voltage integration, but naturally avoids any issues with integrator drift and initial conditions because of the periodic boundary conditions.

$$\Lambda_s\left[k_p\right] = \frac{\mathcal{F}\left\{v_s - R_s \bar{\boldsymbol{i}}_{\boldsymbol{s}}\left[n_p\right]\right\}}{j\left(\omega_p \boldsymbol{K}[k_p] + \omega_e\right)} \tag{10}$$

The frequency scaling parameterω_p, defined by (11), relates the sampling frequency to the cyclic frequency of the period being solved.

$$\omega_p = \frac{2\pi}{T_p} \tag{11}$$

Index $\boldsymbol{K}[k_p]$ is the frequency vector of the DFT, an implementation dependent quantity. Multiplication by $j\omega_p \boldsymbol{K}[k_p]$ is accomplishes a derivative in the frequency domain. The next steps calculate rotor flux $\mathbf{\Lambda_r}[k_p]$ with (12) and $\boldsymbol{I_r}[k_p]$ with (13), giving the complete electrical states of the machine. Note that $\boldsymbol{I_s}\left[k_p\right] = \mathcal{F}\left\{\bar{\boldsymbol{i}}_{\boldsymbol{s}}\left[n_p\right]\right\}$.

$$\mathbf{\Lambda_r}[k_p] = \frac{L_{ar}\mathbf{\Lambda}_{\mathbf{s}}\left[k_p\right] - D\boldsymbol{I_s}\left[k_p\right]}{L_m} \tag{12}$$

$$\boldsymbol{I_r}[k_p] = \frac{L_m \mathbf{\Lambda_s}\left[k_p\right] - L_{as}\mathbf{\Lambda_r}[k_p]}{D} \tag{13}$$

Finally the rotor speed $\widehat{\omega_r}[n_l]$ and motor torque $\widehat{\tau_e}[n_l]$ are computed with (14) and (15), where $n_l = 0, 1, \ldots, N_l - 1$, and N_l is number of points in the longest (or only) periodicity. For a singly periodic case the estimates may be computed directly.

$$\widehat{\omega_r}[n_l] = \frac{2}{P_m}\left(\frac{\dot{\lambda_r}[n_l] + R_r i_r[n_l]}{j\lambda_r[n_l]} + \omega_e\right) \tag{14}$$

$$\hat{\tau}_e[n_l] = \frac{L_m P_m}{2D}\mathbf{Im}\left\{\lambda_s^*[n_l]\,\lambda_r[n_l]\right\} \tag{15}$$

The time derivative of rotor flux, $\dot{\lambda_r}[n_p]$, is obtained by (16).

$$\dot{\boldsymbol{\lambda}}_{\boldsymbol{r}}[n_p] = \mathcal{F}^{-1}\left\{j\omega_p \boldsymbol{K}\left[k_p\right]\boldsymbol{\lambda_r}[n_p]\right\} \tag{16}$$

A multi-periodic case requires special treatment to combine the collection of periodic solutions for $\mathbf{\Lambda_s}n_p$, $\mathbf{\Lambda_r}\left[n_p\right]$, $\dot{\boldsymbol{\lambda}}_{\boldsymbol{r}}\left[n_p\right]$, and $\boldsymbol{i_r}\left[n_p\right]$, each of which may have a different sampling rate. To generate an example signal $x[n_l]$ from its constituent periodicities $\bar{x}\left[n_p\right]$, each periodicity is interpolated to the sampling rate of the longest periodicity, denoted f_{sl}. The interpolation achieves low error by first concatenating copies of $x\left[n_p\right]$ until the vector length is $N_p\left\lfloor N/N_p\right\rfloor$, then zero padding in the frequency domain to a total length of L_l, defined in (17), before inverse DFT. In (17) **round** denotes rounding to the nearest integer.

$$L_l = \mathbf{round}\left(f_{sl}\frac{N_p\left\lfloor N/N_p\right\rfloor}{f_{sp}}\right) \tag{17}$$

The first N_l elements of each concatenated and interpolated periodicity, denoted $x_p\,[n_l]$, are used to construct $x[n_l]$ according to (18), which implements an element-wise removal of the duplicated mean value left in each periodicity by synchronous averaging.

$$x\,[n_l] = \sum_{i=1}^{P} x_i[n_l] - \frac{(P-1)}{PN_l}\sum_{m=0}^{N_l-1}\sum_{i=1}^{P} x_i[n_m] \tag{18}$$

Then (14) and (15) may be computed with the recombined fluxes and rotor currents. $\widehat{\omega_r}[n_l]$ and $\widehat{\tau_e}[n_l]$ are the discrete estimates of $\omega_r(t)$ and $\tau_e(t)$, respectively.

C. Parameter Estimation

Accurate motor parameters are required to compute (10), (11)–(15). Standard methods to measure motor parameters can involve tests at standstill, and generally do not use data under normal operation [42]. This may not reflect the machine state during operation, leading to reduced accuracy in the speed and torque estimates. Parameter error will result in a difference between the mean of the rotor speed estimate, $\bar{\hat{\omega}}_r[n_l]$ and the average of the true rotor speed, $\bar{\omega}_r$, which was previously calculated from the spectrum of the motor currents as a prerequisite to synchronous averaging during data pre-processing. An error function is constructed using the square of the difference. An additional constraint is provided by observing that parameter error will result in imaginary content in $\hat{\omega}_r[n_l]$. The error function is (19), and it depends on the parameter vector θ defined in (20).

$$E(\theta) = \alpha\left(\mathbf{Im}\left(\widehat{\omega_r}[n_l]\right)\right)^2 + \left(\bar{\hat{\omega}}_r - \bar{\omega}_r\right)^2 \tag{19}$$

$$\theta = [R_s, R_r, L_m, L_l] \tag{20}$$

We make the assumption that L_{as} and L_{ar} are equal and construct them by summing L_m and L_l. This guarantees that the stator or rotor total inductance is greater than the magnetizing inductance. The motor's nameplate information can identify the pole pair count P_m. The relative weight of the two error terms on the right hand side of (19) is set by the α term. A trust region reflective Newton algorithm [45] is used to minimize (19), within a $\pm$ one order of magnitude range around the initial guess for each parameter's value.

IV. Experimental Examples and Discussion

This section presents three example induction motor inversion experiments. Section A verifies speed estimation on a direct drive reciprocating compressor, which is an example of the singly-periodic loading case. Section B performs similar inversions on three different multi-periodic loading cases. A fault detection application is described in section C; valve leaks in a reciprocating air-conditioning compressor.

All data presented in this section was processed offline in matlab. Currents and voltages were sampled at LA-55P LEM current transducers and LV-25 voltage transducers, respectively, using a purpose built data acquisition platform developed for non-intrusive load monitoring [46]. Data were sampled at or near 8 kHz. Data records of 30 s to 1 min were recorded, and the 5 to 10 s segment of data with the lowest rms value of instantaneous power variation was selected for synchronous averaging.

A. Singly-Periodic Case

Data were collected from a compressor discharge test rig shown in Fig 4. The compressor's case was drilled and its shaft was extended to install a 2500 cpr optical shaft encoder for verification of the algorithm only. The compressor input was at atmospheric pressure, and the output was attached to a 70 psi pressure regulated air tank to provide a pressure difference across the machine.

The speed comparison in Fig 5a proves that the non-intrusive estimate of $\widehat{\omega_r}[n_l]$, computed with (14) from nothing more than sampled motor currents and voltages, contains the same fine instantaneous angular speed fluctuations of the rotor shaft during one shaft rotation as were measured by a high resolution encoder. In a practical application, without a shaft encoder, it would still be desirable for a user to confirm the accuracy of the estimated $\widehat{\omega_r}[n_l]$ and $\widehat{\tau_m}[n_l]$. Indirect estimate validation can be done by forward simulation of a motor driven by the measured stator voltages and enforcing a rotor speed following $\widehat{\omega_r}[n_l]$. The simulation uses the same model parameters and the resulting simulated currents are compared to the measured stator currents. Fig 5b shows this verification for the compressor discharge experiment. Since the full motor state is recovered as part of the inversion, the simulation's initial conditions are known, as is the electromagnetic torque.

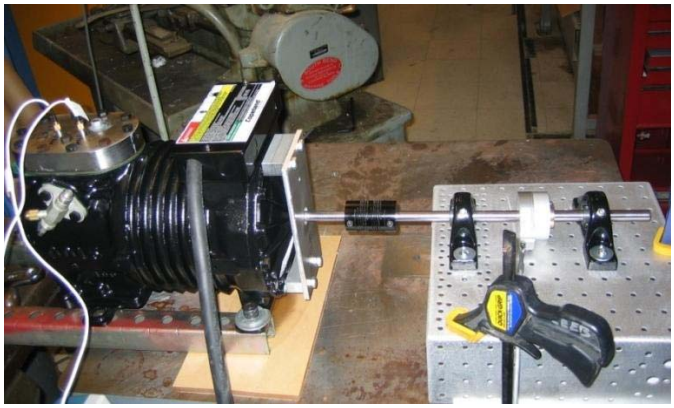

Fig. 4. Compressor test rig with shaft encoder installed on rotor extension.

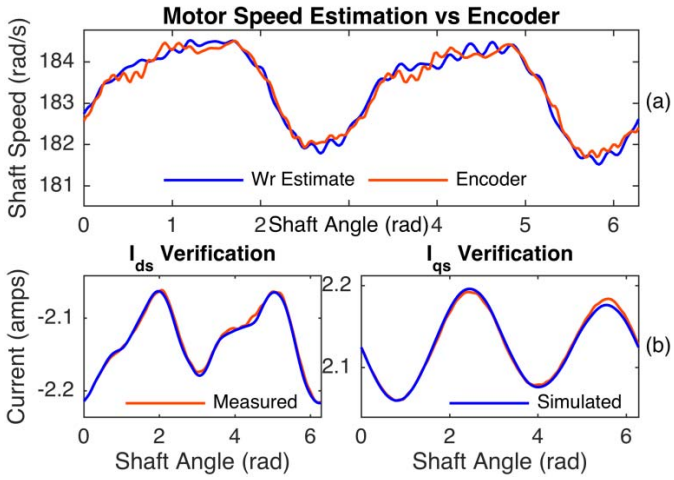

Fig. 5. (a) Speed estimate comparison with encoder measured speed, plotted against mechanical shaft angle. Compressor nominal speed is 1750 rpm. (b) Stator current comparison between measured values and a simulated motor driven with the measured voltages and estimated shaft speed, and using the estimated model parameters.

B. Multi-Periodic Case

Multi-periodic conditions were tested on a three pole pair ventilation fan motor driving a hysteresis dynamometer. The voltage in the dynamometer's breaking coils was modulated by a solid state relay controlled by a signal generator, creating a periodic load torque that is unrelated to the shaft rotation

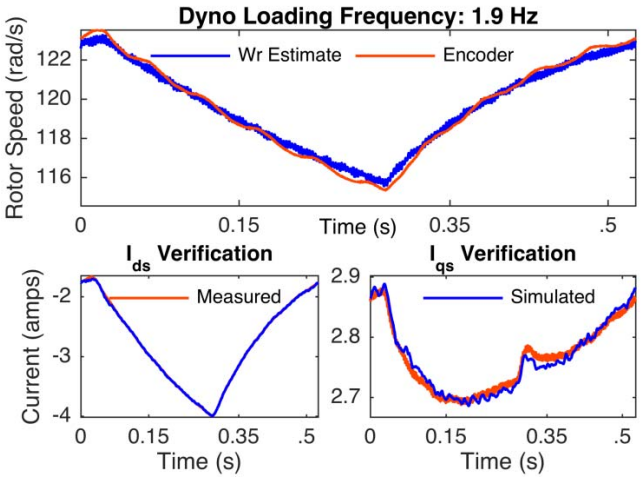

Fig. 6. Long period load torque. Load periodic speed variation is well estimated, but once per-rotation shaft speed variation is not as well recovered.

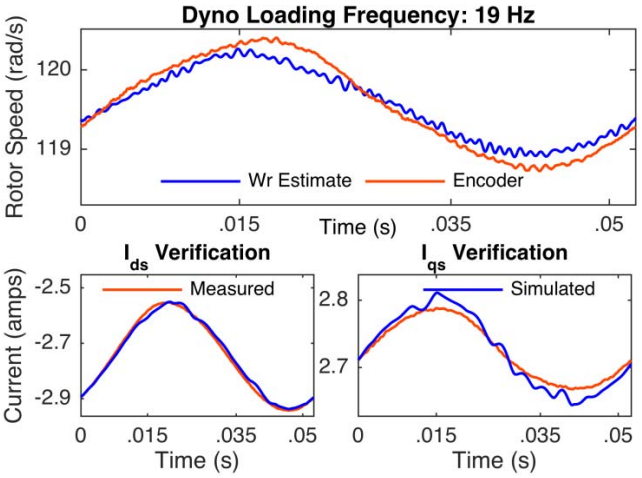

Fig. 7. This case shows load and shaft rotation periodicities within 1 Hz of each other.

speed or angle. A range of load frequencies was tested. Shown are shaft speed estimates and simulated current comparison plots for load frequencies of 1.9 Hz (Fig. 6), 19 Hz (Fig. 7), and 70.8 Hz (Fig 8). The algorithm performs well estimating the shaft speed variation in the multi-periodic case, but not as well the singly periodic case. For this motor, higher number of pole pairs, three pole pairs versus two pole pairs in the compressor motor, means a less sinusoidally distributed magnetic flux than motors with fewer poles, reducing the accuracy of the assumptions inherent in the induction motor model (4)–(6).

Multi-periodic cases also suffer from reduced accuracy if the rotor rotation period is continually changed by a dominating external load, as in Fig. 6. Variation in the shaft rotation period caused by periodic but non-shaft-synchronous load torque will result in spectral smearing of the shaft rotation harmonics. This smearing leads to some information loss during synchronous averaging, and can cause reduced inversion accuracy.

C. Reciprocating Compressor Valve Fault

Reciprocating compressor valve fault detection shows the value direct time domain examination of an estimated load

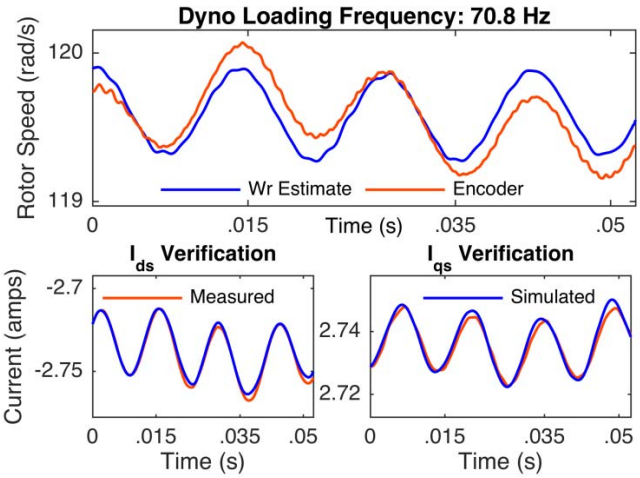

Fig. 8. Fast load variation. Again load linked speed variation is well estimated and the once per-shaft rotation variation in speed is not as well estimated.

torque signal. Causes of damage include attempted compression of incompressible material such as condensed gas, refrigerant, oil, or interaction with solid debris in the refrigeration loop [47]. Corrosion and fatigue can also damage valves. Damaged or leaky valves do not effectively seal the compression cylinder from the suction or discharge manifolds, causing a loss of volumetric efficiency for the compressor [48]. As a soft fault in an otherwise hard to diagnose and sense location, compressor valve faults are an ideal target for the motor inversion based condition monitoring.

We studied a two piston compressor with reed type suction and discharge valves. Photographs of failed reed valves in [47] were used as a guide to intentionally damage suction reeds in a functionally similar manner, shown for our experiments in Fig. 9a. Four test reeds were used, corresponding to a leak-free baseline and three faulty suction reeds of increasing leak size. For the four experiments, one of the compressor's cylinders always un-modified leak free valves, while the other cylinder received one of the four test reeds. After each valve installation, shown in Fig 9b and Fig. 9c, the air conditioner system was re-charged with refrigerant and allowed to run for approximately 5-10 minutes to settle the air condition start up transient. Then a one minute period of voltage and current data were recorded for processing. Cylinder pressure measurements were also collected with high dynamic range pressure sensors installed in the compressor head plate to assess the severity of the leak on the cylinder pressure waveform [35].

D. Results

From the $\omega_r(t)$ and $\tau_e(t)$ estimates of the motor inversion procedure, (1) was solved to give the load torque $\tau_l(t)$, assuming constant inertia of the rotating components. The minor angle dependence of the mechanism's inertia and the small centrifugal torque component in the slider crank equations of motion [4], are ignored as these components are small for this compressor's geometry and operational speed. $\tau_l(t)$ is primarily composed of friction and pressure torques, and is sensitive to mechanical faults. Each large pulse of the load torque curve corresponds to a particular piston due to the dominant contribution of that piston's pressure torque during

Fig. 9. (a) Test suction reeds showing a leak free reed and three leak reeds. (b) Reeds installed in compressor head over pistons. (c) Leakage holes are located over the suction port.

TABLE I
CYLINDER FAULT SEVERITY METRIC

Suction Valve Hole Area	Fault Detection Metric
Baseline (no hole)	0.74
0.8 mm^2	5.46
1.5 mm^2	8.66
3.1 mm^2	11.92

the compression and discharge phase of its cycle. When one piston is in its compression and discharge stroke, the other piston is in an expansion and fill stroke, with nearly equal pressures across the piston and negligible contribution to the load torque. This property allows each load torque pulse (two per shaft revolution) to be assigned to a cylinder. A healthy symmetrical two cylinder compressor, should have symmetrical load torque pulses, each cylinder pressure torque should be indistinguishable from the other cylinder. Therefore we take the step of superimposing each cylinder's load torque pulse in Fig. 10. The plots in Fig. 10 are normalized and have the sign convention that positive load torque accelerates the crankshaft.

The degree of dissimilarity between each cylinder's load torque pulse increases with the severity of the valve leak in Fig. 10b-d. From the matching overlaid pressure sensor traces in Fig 11a-d, it is clear that the suction valve leak reduces the pressure in the affected cylinder, reducing the load torque when the affected cylinder undergoes compression. A simple metric that captures the dissimilarity between each cylinder's load torque curve is the difference in area enclosed by each curve, tabulated in table I. This metric should be sensitive to discharge valve faults and other leaks, such as gasket or seal leaks, using an identical procedure. A necessary

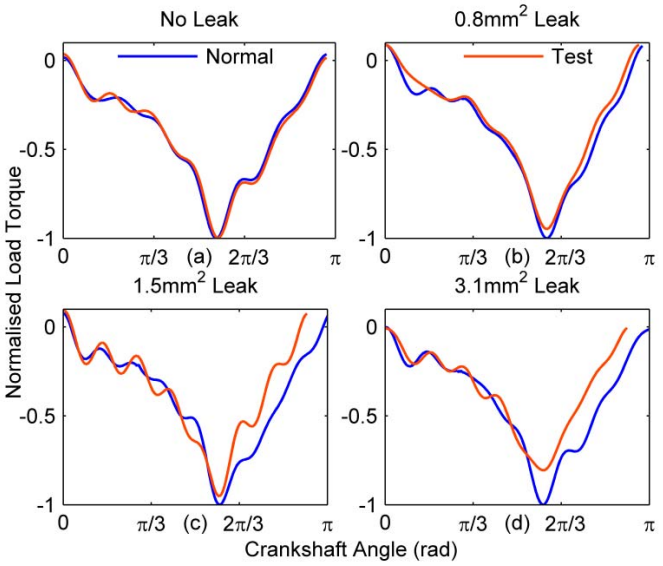

Fig. 10. (a)-(d) Normalized load torque curves associated with each cylinder's compression and discharge stroke. The test reed cylinder's load torque pulsation is superimposed on the healthy cylinder's torque pulsation so that symmetry differences are easy to determine.

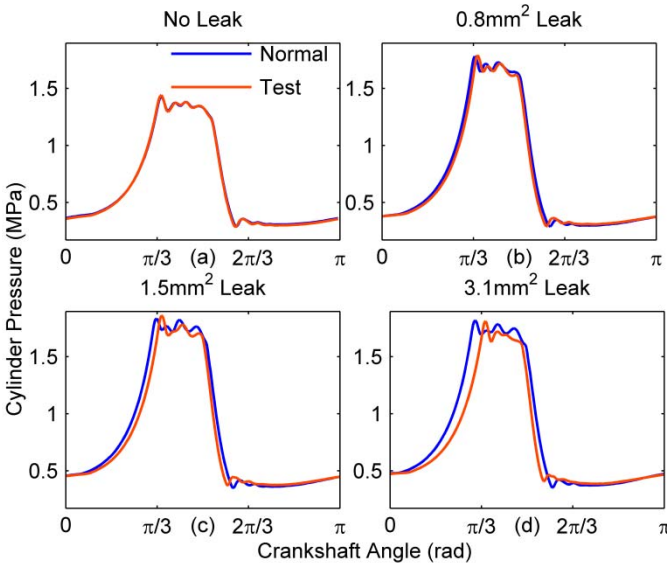

Fig. 11. (a)-(d) Cylinder pressure measurements show test cylinder at lower pressure than normal cylinder due to suction valve leaks.

assumption for this procedure is that the fault affects one cylinder to a greater degree than the other cylinder. If this is not the case in a given machine, comparisons to pre-recorded baselines at known operating conditions can be employed for fault detection.

E. Discussion

This method is directed to subtle faults that can be identified during periodic operation. Not all faults are this way, e.g. arcing or other transient occurrences in the motor or load, but many faults are periodic. While the method's estimation of resistances and inductances can be of some value to detection of some motor related faults, significant motor electrical faults would invalidate the model inversion portion of the method

as the assumed symmetric motor model dynamics would no longer apply. However, many of the procedures that exist in the literature for motor electric fault detection would not require additional instrumentation or signal measurement beyond that required for the present method, and so could be implemented in parallel to the computation of the present paper to perform motor electrical fault detection.

Our aim is transform a healthy induction motor driving a periodic load into its own virtual speed and torque sensor. With the recovered speed and torque signals, any number of criteria may be constructed to determine various fault conditions of a wide and disparate variety of attached periodic loads. In general there would be no one criterion that works for every load or fault of interest. However, a general approach of trending the recorded speed and torque signatures of a given load over time, and periodic comparison of speed and torque signatures against known historical "good" signatures under the same operating conditions, is expected to provide indication of fault related changes in the signatures. Setting the right threshold of deviation to declare a fault would be application and load specific.

In real applications, a data acquisition system measuring and storing the three current and three voltage signals at a sufficient bandwidth would be required. While the method is not immediate or real-time due to the requirement to perform the synchronous averaging of a sufficiently long record of measured signals to suppress the noise and unmodeled dynamics, after the averaging window is established the method can compute quickly and give results in near real time. Computation could be implemented in a motor control DSP, requiring no extra offline computational hardware, if desired.

V. Conclusion

This paper presents an algorithm and data processing steps to monitor the load condition from the motor terminals, in the case of motors operating in periodic-steady state. The result is a high fidelity estimate of shaft speed and electromagnetic torque suitable for computation of the inertia torque and load torque, thereby rendering the motor transparent to the load condition information in the load torque signal. The method provides a parameter estimation step so that deep *a priori* knowledge of the motor parameters is not a requirement. The direct use of time domain load torque eases fault diagnosis, compared to the tracking of spectral frequencies in stator currents or the electromagnetic torque. Experimental validation of the method's speed estimate shows performance similar to a high resolution optical shaft encoder. The inversion method is extended to the multi-periodic loading conditions. The detection of load torque pulsation asymmetry arising from leaks in the valves of a reciprocating compressor illustrates the utility of the method for determining developing fault pathologies in industrially and commercially relevant loads.

References

[1] P. Waide and C. U. Brunner, *Energy-Efficiency Policy Opportunities for Electric Motor-Driven Systems*. Paris, France: International Energy Agency, 2011.

[2] C. Schantz and S. B. Leeb, "Non-intrusive fault detection in reciprocating compressors," in *Proc. 14th Int. Refrig. Air Conditioning Conf. Purdue.*, West Layfette, IN, USA, 2012, pp. 1–10.

[3] P. C. Krause, O. Wasynczuk, S. D. Sudhoff, and S. Pekarek, *Analysis of Electric Machinery and Drive Systems*, Hoboken, NJ, USA: Wiley, 2013.

[4] Y. Kurihara, T. Kaburagi, and K. Watanabe, "Room ventilation control by a self-sensing fan," *IEEE Sensors J.*, vol. 16, no. 7, pp. 2094–2099, Apr. 2016.

[5] C. C. Lin and N. C. Tsai, "Air-gap detection circuit using equivalent capacitive changes for inductive micromotor," *IEEE Sensors J.*, vol. 15, no. 3, pp. 1611–1623, Mar. 2015.

[6] J. Zhang, Y. Chang, and Z. Xing, "Study on self-sensor of linear moving magnet compressor's piston stroke," *IEEE Sensors J.*, vol. 9, no. 2, pp. 154–158, Feb. 2009.

[7] C.-S. Liu and H.-F. Li, "Design and experimental validation of novel force sensor," *IEEE Sensors J.*, vol. 15, no. 8, pp. 4402–4408, Aug. 2015.

[8] S. Nandi, H. A. Toliyat, and X. Li, "Condition monitoring and fault diagnosis of electrical motors—A review," *IEEE Trans. Energy Convers.*, vol. 20, no. 4, pp. 719–729, Dec. 2005.

[9] P. Zhang, Y. Du, T. G. Habetler, and B. Lu, "A survey of condition monitoring and protection methods for medium-voltage induction motors," *IEEE Trans. Ind. Appl.*, vol. 47, no. 1, pp. 34–46, Jan./Feb. 2011.

[10] A. Siddique, G. S. Yadava, and B. Singh, "A review of stator fault monitoring techniques of induction motors," *IEEE Trans. Energy Convers.*, vol. 20, no. 1, pp. 106–114, Mar. 2005.

[11] M. R. Mehrjou, N. Mariun, M. H. Marhaban, and N. Misron, "Rotor fault condition monitoring techniques for squirrel-cage induction machine—A review," *Mech. Syst. Signal Process.*, vol. 25, no. 8, pp. 2827–2848, Nov. 2011.

[12] A. Bellini, F. Filippetti, C. Tassoni, and G. A. Capolino, "Advances in diagnostic techniques for induction machines," *IEEE Trans. Ind. Electron.*, vol. 55, no. 12, pp. 4109–4126, Dec. 2008.

[13] T. G. Habetler, "Effects of time-varying loads on rotor fault detection in induction machines," *IEEE Trans. Ind. Appl.*, vol. 31, no. 4, pp. 900–906, Jul. 1995.

[14] M. Blodt, J. Regnier, and J. Faucher, "Distinguishing load torque oscillations and eccentricity faults in induction motors using stator current Wigner distributions," *IEEE Trans. Ind. Appl.*, vol. 45, no. 6, pp. 1991–2000, Nov./Dec. 2009.

[15] C. Kral, T. G. Habetler, and R. G. Harley, "Detection of mechanical imbalances of induction machines without spectral analysis of time-domain signals," *IEEE Trans. Ind. Appl.*, vol. 40, no. 4, pp. 1101–1106, Jul. 2004.

[16] S. Mukhopadhyay and S. Chaudhuri, "A feature-based approach to monitor motor-operated valves used in nuclear power plants," *IEEE Trans. Nucl. Sci.*, vol. 42, no. 6, pp. 2209–2220, Dec. 1995.

[17] S. Rajagopalan, T. G. Habetler, R. G. Harley, T. Sebastian, and B. Lequesne, "Current/voltage-based detection of faults in gears coupled to electric motors," *IEEE Trans. Ind. Appl.*, vol. 42, no. 6, pp. 1412–1420, Nov./Dec. 2006.

[18] C. Kar and A. R. Mohanty, "Monitoring gear vibrations through motor current signature analysis and wavelet transform," *Mech. Syst. Signal Process.*, vol. 20, no. 1, pp. 158–187, Jan. 2006.

[19] A. R. Mohanty and C. Kar, "Fault detection in a multistage gearbox by demodulation of motor current waveform," *IEEE Trans. Ind. Electron.*, vol. 53, no. 4, pp. 1285–1297, Jun. 2006.

[20] S. H. Kia, H. Henao, and G.-A. Capolino, "Gearbox monitoring using induction machine stator current analysis," in *Proc. IEEE SDEMPED*, Cracow, Poland, Sep. 2007, pp. 149–154.

[21] S. H. Kia, H. Henao, and G. A. Capolino, "Analytical and experimental study of gearbox mechanical effect on the induction machine stator current signature," *IEEE Trans. Ind. Appl.*, vol. 45, no. 4, pp. 1405–1415, Jul. 2009.

[22] M. Blodt, M. Chabert, J. Regnier, and J. Faucher, "Mechanical load fault detection in induction motors by stator current time-frequency analysis," *IEEE Trans. Ind. Appl.*, vol. 42, no. 6, pp. 1454–1463, Nov./Dec. 2006.

[23] M. Blodt, D. Bonacci, J. Regnier, M. Chabert, and J. Faucher, "On-line monitoring of mechanical faults in variable-speed induction motor drives using the Wigner distribution," *IEEE Trans. Ind. Electron.*, vol. 55, no. 2, pp. 522–533, Feb. 2008.

[24] M. Blodt, P. Granjon, B. Raison, and J. Regnier, *Mechanical Fault Detection in Induction Motor Drives Through Stator Current Monitoring—Theory and Application Examples*, 2010. [Online]. Available: http://www.intechopen.com/books/faultdetection/

[25] R. Yacamini, K. S. Smith, and L. Ran, "Monitoring torsional vibrations of electro-mechanical systems using stator currents," *Trans. ASME, J. Vib. Acoust.*, vol. 120, no. 1, pp. 72–79, Jan. 1998.
[26] S. H. Kia, H. Henao, and G.-A. Capolino, "Non-stationary condition torsional vibration monitoring using induction machine electromagnetic torque estimation," in *Proc. ICEM*, Vilamoura, Portugal, Sep. 2008, pp. 1–7.
[27] S. H. Kia, H. Henao, and G.-A. Capolino, "Torsional vibration assessment in railway traction system mechanical transmission," in *Proc. IEEE SDEMPED*, Cargese, France, Aug. /Sep. 2009, pp. 1–8.
[28] S. H. Kia, H. Henao, and G.-A. Capolino, "Torsional vibration effects on induction machine current and torque signatures in gearbox-based electromechanical system," *IEEE Trans. Ind. Electron.*, vol. 56, no. 11, pp. 4689–4699, Nov. 2009.
[29] S. H. Kia, H. Henao, and G.-A. Capolino, "Torsional vibration assessment using induction machine electromagnetic torque estimation," *IEEE Trans. Ind. Electron.*, vol. 57, no. 1, pp. 209–219, Jan. 2010.
[30] H. Henao, S. H. Kia, and G.-A. Capolino, "Torsional-vibration assessment and gear-fault diagnosis in railway traction system," *IEEE Trans. Ind. Electron.*, vol. 58, no. 5, pp. 1707–1717, May 2011.
[31] I. X. Bogiatzidis, A. N. Safacas, and E. D. Mitronikas, "Detection of backlash phenomena appearing in a single cement kiln drive using the current and the electromagnetic torque signature," *IEEE Trans. Ind. Electron.*, vol. 60, no. 8, pp. 3441–3453, Aug. 2013.
[32] B. Trajin, J. Regnier, and J. Faucher, "Comparison between stator current and estimated mechanical speed for the detection of bearing wear in asynchronous drives," *IEEE Trans. Ind. Electron.*, vol. 56, no. 11, pp. 4700–4709, Nov. 2009.
[33] C. R. Laughman, "Fault detection methods for vapor compression air conditioners using electrical measurements," Ph.D. dissertation, Dept. Arch., Massachusetts Inst. Technol., Cambridge, MA, USA, 2008.
[34] Z. Gao, L. Turner, R. S. Colby, and B. Leprettre, "A frequency demodulation approach to induction motor speed detection," *IEEE Trans. Ind. Appl.*, vol. 47, no. 4, pp. 1632–1642, Jul./Aug. 2011.
[35] A. Ferrah *et al.*, "A speed identifier for induction motor drives using real-time adaptive digital filtering," *IEEE Trans. Ind. Appl.*, vol. 34, no. 1, pp. 156–162, Jan. 1998.
[36] E. Delaleau and A. M. Stankovic, "Modeling and simulation of the induction motor with position-dependent load torque," in *Proc. 42nd CDC.*, vol. 6, Dec. 2003, pp. 6212–6217.
[37] T. Vikopoulos, "Induction motors in electromechanical systems with a periodical moment of inertia—Analytical calculation of forced oscillations and test. Part 1," *Arch. Elektrotech.*, vol. 68, no. 3, pp. 211–216, 1985.
[38] T. Vikopoulos, "Induction motors in electromechanical systems with a periodical moment of inertia—Analytical calculation of forced oscillations and test. Part 2," *Arch. Elektrotech.*, vol. 68, no. 3, pp. 217–222, 1985.
[39] H. Engl, H. Werner, M. Hanke, and A. Neubauer, *Regularization of Inverse Problems*. Dordrecht, The Netherlands: Kluwer, 2000.
[40] C. Schantz, "Non-intrusive Fault Detection in Reciprocating Compressors," Ph.D. dissertation, Dept. Mech. Eng., Massachusetts Inst. Technol., Cambridge, MA, USA, 2014.
[41] W. Lohmiller and J.-J. E. Slotine, "On contraction analysis for non-linear systems," *Automatica*, vol. 34, no. 6, pp. 683–696, 1998.
[42] S. Braun, "The synchronous (time domain) average revisited," *Mech. Syst. Signal Process.*, vol. 25, no. 4, pp. 1087–1102, May 2011.
[43] H. A. Toliyat, E. Levi, and M. Raina, "A review of RFO induction motor parameter estimation techniques," *IEEE Trans. Energy Convers.*, vol. 18, no. 2, pp. 271–283, Jun. 2003.
[44] T. F. Coleman and Y. Li, "An interior trust region approach for nonlinear minimization subject to bounds," *SIAM J. Optim.*, vol. 6, no. 2, pp. 418–445, 1996.
[45] S. R. Shaw, S. B. Leeb, L. K. Norford, and R. W. Cox, "Nonintrusive load monitoring and diagnostics in power systems," *IEEE Trans. Instrum. Meas.*, vol. 57, no. 7, pp. 1445–1454, Jul. 2008.
[46] W. A. Glaeser, "Failure mechanisms of Reed valves in refrigeration compressors," *Wear*, vols. 225–229, pp. 918–924, Apr. 1999.
[47] M. S. Breuker and J. E. Braun, "Common faults and their impacts for rooftop air conditioners," *Int. J. HVAC&R Res.*, vol. 4, no. 3, pp. 303–318, 1998.
[48] B. Paul, *Kinematics and Dynamics of Planar Machinery*. Englewood Cliffs, NJ, USA: Prentice-Hall, 1979.

Christopher J. Schantz received the B.S. degree in mechanical engineering from the California Institute of Technology in 2008, and the M.S. and Ph.D. degrees from the Massachusetts Institute of Technology, in 2011 and 2014, respectively. He was a Senior Engineer with Tesla Motors. He is currently with Lockheed Martin. (Tesla Motors and Lockheed Martin not affiliated with this research). His research interest lies in signal processing for sensing and control systems.

Steven B. Leeb received the Ph.D. degree from the Massachusetts Institute of Technology (MIT) in 1993. He has been a Faculty Member with the Department of Electrical Engineering and Computer Science, MIT, since 1993. He holds a joint appointment in MIT's Department of Mechanical Engineering. He is concerned with the development of signal processing algorithms for energy and real-time control applications.